A Portable FMCW Interferometry Radar With Programmable Low-IF Architecture for Localization, ISAR Imaging, and Vital Sign Tracking

Zhengyu Peng, *Student Member, IEEE*, José María Muñoz-Ferreras, *Member, IEEE*, Yao Tang, *Student Member, IEEE*, Chenhui Liu, *Student Member, IEEE*, Roberto Gómez-García, *Senior Member, IEEE*, Lixin Ran, and Changzhi Li, *Senior Member, IEEE*

***Abstract*— This paper presents a portable radar system for short-range localization, inverse synthetic aperture radar imaging, and vital sign tracking. The proposed sensor incorporates frequency-modulated continuous-wave (FMCW) and interferometry (Doppler) modes, which enable this radar system to obtain both absolute range information and tiny vital signs (i.e., respiration and heartbeat) of human targets. These two different operation modes can be switched through an on-board microcontroller. To simplify the system, the proposed radar utilizes the audio card of a laptop to sample the baseband signal. The FMCW mode of the radar uses operational-amplifier-based circuits to generate an analog sawtooth signal and a reference pulse sequence (RPS). The RPS is locked to the sawtooth signal to obtain coherence for the radar system. For the interferometry mode, a low-intermediate-frequency modulation method is implemented to avoid the slow vital signs from being distorted by the high-pass filter of the audio card. Several experiments were carried out to reveal the capability and distinct operational features of the proposed portable hybrid radar. The experiments also showed that the system can easily detect glass, which is usually difficult to identify for optical-based sensors. In addition, 2-D scanning in a complex environment revealed that the proposed radar was able to differentiate human targets from other objects. Moreover, ISAR images were used to isolate moving human targets from surrounding clutter. Finally, the proposed radar also demonstrated its ability to accurately measure vital signs when a human subject sits still.**

***Index Terms*— Frequency-modulated continuous-wave (FMCW) radar, hybrid operation mode, interferometry radar, inverse synthetic aperture radar (ISAR), low-intermediate-frequency (low-IF), vital Doppler information, vital sign measurement.**

I. Introduction

SHORT-RANGE localization and vital sign tracking are two hot research topics in the fields of consumer electronics, medical care surveillance, driver assistance, and indoor navigation for robots and drones. In these applications, microwave radar systems have their intrinsic advantages compared with conventional contact-required sensors or camera-based solutions. Contact-based sensors such as transducers may make people feel uncomfortable after wearing them for a long time, which limits the applications of these kinds of devices. Camera-based alternatives such as widely used surveillance cameras have the ability to monitor and track targets from a distance. Moreover, recent technologies such as the Kinect [1] from Microsoft and the Project Tango from Google enable cameras to obtain depth images. Regardless of the success in depth sensing [2]–[4], camera-based approaches still suffer from some important problems. One of the most severe shortcomings of these sensors is that they highly rely on light, which may be changing from time to time. For example, in vehicular environments, it is quite common that light varies suddenly at night when a vehicle occasionally directs its high-beam toward the camera, leading to its blinding for a short period of time. Additionally, camera-based sensors can be easily blocked by obstacles, or in other cases, they cannot detect transparent obstacles such as glass. The challenge for camera-based sensors to detect glass is prevalent in applications such as driver assistance and robot/drone indoor navigation, since glass is widely used for doors and walls in modern buildings. A robot or a drone may crash into glass if its sensor fails to find the existence of glass obstacles. Hyperspectral imaging systems [5] enable sensors to

Manuscript received March 11, 2016; revised July 20, 2016 and November 21, 2016; accepted November 21, 2016. Date of publication December 15, 2016; date of current version April 3, 2017. This work was supported in part by the National Science Foundation (NSF) under Grant ECCS-1254838, in part by the National Natural Science Foundation of China (NSFC) under Grant 61528104, Grant 61131002, and Grant 61071063, in part by the University of Alcalá under Project CCG-2015=EXP-017, and in part by the Spanish Ministry of Economy and Competitiveness under Project TEC2014-54289-R.

Z. Peng, Y. Tang, and C. Li are with the Department of Electrical and Computer Engineering, Texas Tech University, Lubbock, TX 79409 USA (e-mail: zhengyu.peng@ttu.edu; changzhi.li@ttu.edu).

J. M. Muñoz-Ferreras and R. Gómez-García are with the Department of Signal Theory and Communications, University of Alcalá, 28871 Madrid, Spain.

C. Liu is with Qualcomm, San Jose, CA 95110 USA.

L. Ran is with the Laboratory of Applied Research on Electromagnetics, Zhejiang University, Hangzhou 310027, China.

This paper has supplementary downloadable material available at http://ieeexplore.ieee.org, provided by the authors. The supplementary file contains a video that illustrates the real-time ISAR imaging of two human subjects walking in a corridor using the proposed portable hybrid radar in the FMCW mode. As noted in the paper, the audio card in a laptop was used to sample the data. Real-time signal processing was implemented in National Instruments (NI) LabVIEW. The file size is 61.6 MB.

Color versions of one or more of the figures in this paper are available online at http://ieeexplore.ieee.org.

Digital Object Identifier 10.1109/TMTT.2016.2633352

identify the material property of an object and are widely used in astronomy, agriculture, biomedical imaging, geosciences, physics, and surveillance. However, these systems suffer from problems common to conventional camera-based methods, such as difficulty in penetrating obstacles, and they are very expensive and complicated. On the contrary, microwave radars do not rely on light and can easily penetrate walls and obstacles [6]–[9]. It is also easy for radars to detect the existence of glass. Furthermore, radar sensors are much more sensitive to vital signs [9]–[12], and they can also reveal extra details of motion based on Doppler and micro-Doppler characteristics [13]–[16].

Continuous-wave (CW) radars have advantages of low transmitted power, simple structure, and high sensitivity, which make their applications spread into various areas. Typically, there are two types of CW radars: 1) unmodulated CW systems and 2) modulated CW solutions. An interferometry (Doppler) radar is a kind of unmodulated CW system [17]–[19]. It operates based on a single-tone CW to obtain phase history of targets. In addition, this kind of radar features high precision in displacement and speed measurement [9], [12], [20]. However, it has difficulty to get absolute range information of targets. Modulated CW radars include frequency-shift keying radar [21], stepped frequency CW radar [22], and frequency-modulated CW (FMCW) radar [23]–[27]. The FMCW radar is one of the most popular types. With FMCW radar sensors, it is easy and inexpensive to obtain accurate range information of targets. In addition, FMCW radars can extract Doppler information related to the target radial velocity and measure displacements of targets if the coherence property of the system is achieved [28]. It is worth noting that the hardware and signal processing for an FMCW system measuring displacements are much more complex than those for unmodulated CW systems. Moreover, the displacement accuracy of an FMCW radar may not be as good as that of unmodulated CW systems, which can easily achieve submillimeter accuracy [28]. By making the radar coherent, the phase history of the targets is preserved during the coherent processing interval (CPI) and Doppler information can thus be derived, which provides two dimensions: the range and the Doppler. This 2-D information can help to isolate the wanted moving targets from surrounding stationary clutter [29]–[33]. With this idea, a 5.8-GHz FMCW radar was used to isolate a moving human subject from surrounding stationary clutter in [32]. The same method was also implemented in a 24-GHz prototype [33]. However, for FMCW radars, a finer range resolution needs a larger transmitted bandwidth [34]. Thus, the operation frequency of small-fractional-bandwidth radar systems must be high enough to meet resolution requirements [40]. This frequency increase leads to great efforts in order to minimize system cost and complexity.

In this paper, a portable FMCW interferometry radar is proposed, whose operation frequency is at 5.8 GHz. The proposed radar system can be configured in either the FMCW or interferometry mode by means of an on-board microcontroller. Compared with [41], whose hardware system was based on bulky instruments, and a low-cost and portable solution is proposed in this paper. To simplify the system complexity and minimize its cost, the two radar modes are realized to share the same RF components and signal paths. In addition, at the signal acquisition block, the audio card of a laptop is used to sample the baseband signal. On the other hand, the interferometry mode operates at a single frequency of 5.8 GHz. It is known that vital signs, i.e., respiration and heartbeat, are extreme low-frequency signals, which can be easily blocked by the bandpass filter of an audio card [42]. In this paper, a low-intermediate-frequency (low-IF) modulation method is implemented to upconvert the baseband signal to an IF, so that the tiny low-frequency vital signs will not be filtered out by the audio card [42]. Note also that the low-IF scheme has advantages in relation to mitigation of flicker noise, which has a higher power level at the around-zero-frequency components of the baseband signal. After data acquisition, envelope detection is proposed here to recover the vital signs in the interferometry mode. The distortion effect of low-IF modulation and the way to optimize the sensitivity of envelope detection are analyzed. Regarding the FMCW mode, a free-running voltage-controlled oscillator (VCO) controlled by a simple operational-amplifier-based circuit is used to generate the desired frequency-modulated RF signal. By acquiring the baseband output along with a reference pulse sequence (RPS), which is locked to the sawtooth signal, the coherence property of the radar can be achieved.

With this engineered portable hybrid radar, several experiments were carried out. First, the radar was used to detect the existence of glass in the FMCW mode. Then, an experiment was performed to differentiate a human target from strong stationary clutter returns, which is a challenge especially when the human is not moving. Further FMCW mode experiments enabled to derive real-time inverse synthetic aperture radar (ISAR) images [29]–[31] to track the echoes of two walking pedestrians in the 2-D range Doppler domain. Finally, human respiration and heartbeat rates were measured by the prototype in the interferometry mode with the suggested low-IF modulation and envelope detection processes.

This paper is organized as follows. Section II presents the design principles of the proposed portable hybrid radar system. In Section III, several experiments are described, showing the capabilities and operational performance of the prototype in short-range localization and vital sign tracking. Finally, main conclusions of this paper are summarized in Section IV.

II. Portable Hybrid Radar

This section reports the architecture, theoretical foundations, and design aspects of the conceived portable radar system.

A. System Design

Fig. 1 details the block diagram of the proposed portable FMCW interferometry hybrid radar system. The two different radar modes share most of the RF components and signal paths. Analog switches are used to set up the radar in one of the two operational modes, and all the analog switches are configured by an on-board microcontroller. For the FMCW mode, the mode switches are turned to the

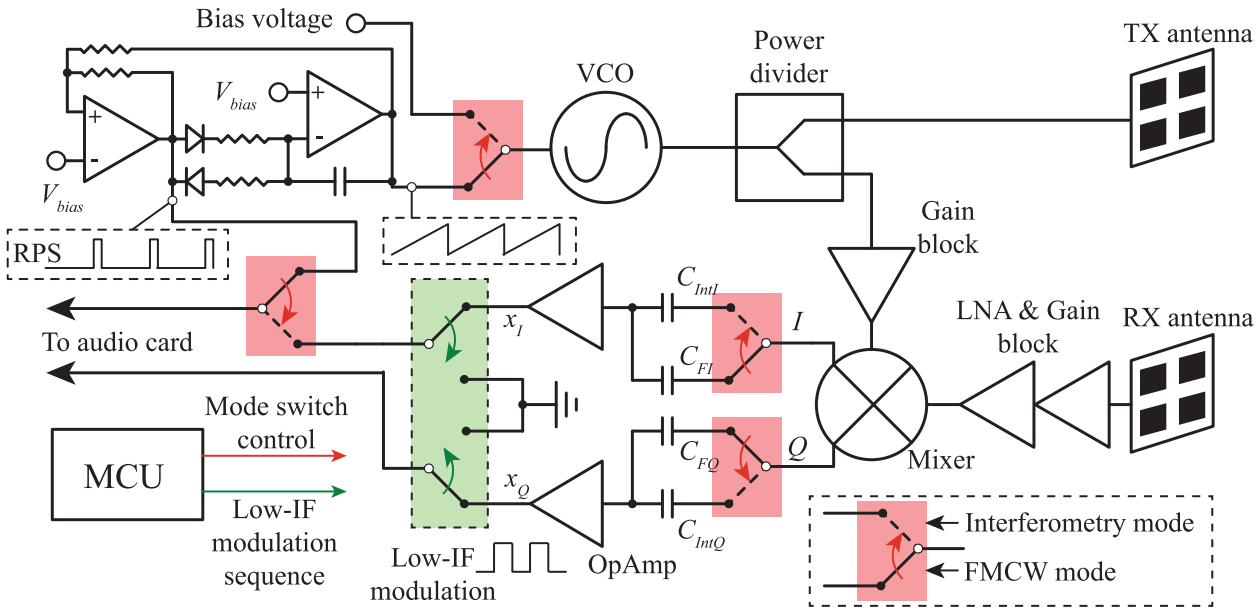

Fig. 1. Block diagram of the portable FMCW interferometry radar system.

solid line in Fig. 1. The theory of FMCW radars has already been detailed in previous works (see [34]). In a conventional design, a frequency synthesizer, usually consisting of a combination of a direct digital synthesizer and a phase-locked loop (PLL) [23]–[25], [35], or based on a highly integrated fractional-N PLL [36], is required to generate the frequency ramps, which leads to an increase in complexity and cost of the whole system.

In the conceived radar prototype, which aims at portability and low cost, a simple operational-amplifier-based circuit is employed to generate the sawtooth ramp voltage, which is used to tune a free-running VCO to generate the frequency ramps [37]. The operational-amplifier-based circuit also simultaneously synthesizes the RPS, which is locked to the sawtooth ramp voltage signal. The frequency of these sawtooth ramp voltages and RPS signals is 82 Hz in the implemented prototype. The bandwidth of the transmitted signal is 320 MHz with a center frequency around 5.8 GHz, and the transmitted average power is 8 dBm. On the receiver channel, two small capacitors, C_{FI} and C_{FQ} (20 nF in the prototype), are used to block the dc and near-field coupling between antennas. In the acquisition stage of the FMCW mode, only the Q channel baseband signal x_Q and the RPS are sampled by a two-channel audio card.

Conventionally, VCOs have problems in linearity, and linearity requirement becomes more stringent with an increasing range [37]–[39]. However, the applications of the proposed radar system focuses on short range, i.e., within 20 m. The degradation of the range resolution due to the VCO linearity issue is not significant. In order to clearly illustrate the effect of the nonlinear tuning curve, a simulation based on the tuning curve of the actual VCO used in the proposed system was performed.

Fig. 2 shows the frequency versus tuning voltage curve of the VCO used in this paper. A third-order polynomial is used

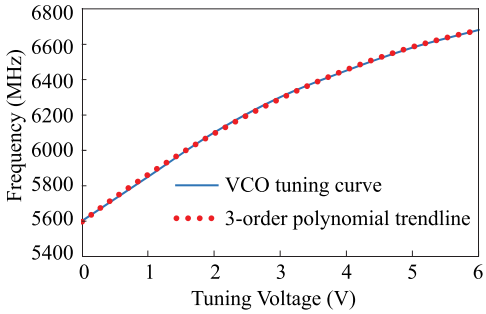

Fig. 2. VCO output frequency versus tuning voltage.

to fit this voltage tuning curve, which leads to

$$f_{\mathrm{VCO}} = 2 \times 10^{-12} V_t^3 - 17.3 V_t^2 + 283.9 V_t + 5595.5 \qquad (1)$$

where f_{VCO} (in megahertz) is the output frequency of the VCO and V_t (in volts) is the tuning voltage. The tuning voltage V_t was swept from 0.15 V to 1.4 V, corresponding to an output frequency bandwidth of 320 MHz. Fig. 3 shows the comparison of the range profiles between the VCO used in the proposed design and an ideal VCO with a linear tuning curve. Fig. 3(a) and (b) shows the simulated results with the point target at the 10-m range and the target at the 15-m range, respectively. The degradation in range resolution can be observed for the realistic VCO, while the absolute range can still be accurately measured. This degradation in range resolution is acceptable for the proposed localization applications, and is worthwhile considering the cost and complexity of implementing a PLL-based signal synthesizer.

When the radar is changed to the interferometry (Doppler) mode, i.e., the mode switches are turned to the dashed lines in Fig. 1, the input to the VCO is a constant control voltage

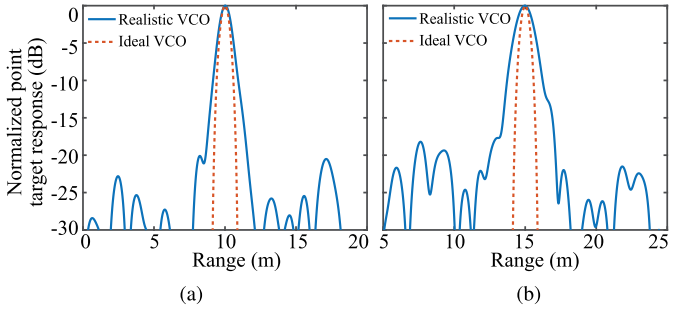

Fig. 3. Simulated range profiles of a point target with an ideal VCO and arealistic VCO used in this design. (a) 10-m range. (b) 15-m range.

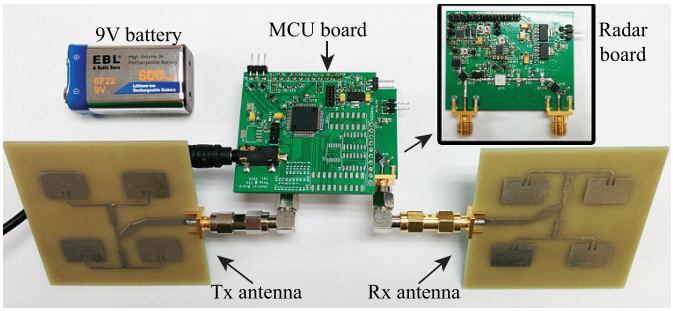

Fig. 4. Photograph of the radar prototype.

so that the generated single-tone frequency is around 5.8 GHz. On the receiver channel after the mixer, two large capacitors, $C_{\mathrm{Int}I}$ and $C_{\mathrm{Int}Q}$ (10 μF in the prototype), are used to block the dc component [43], [44] of the I/Q signals. This results in a simplification of the dc offset configuration for the baseband amplifiers. Large capacitors are necessary here to minimize the distortion of the extremely low-frequency vital signs. After being amplified by the baseband amplifiers, the signals in the I/Q channels, i.e., x_I and x_Q, are modulated with the low-IF digital local oscillator, which is realized through the low-IF switches in Fig. 1 operated by the microcontroller with a constant frequency of 32 Hz. Then, the two-channel modulated signals are sampled by the audio card. Note that the principle of operation for interferometry radars can be found in [34].

Fig. 4 details the photograph of the implemented portable hybrid radar system. The prototype consists of two printed circuit boards stacked together. The top and bottom of Fig. 4 are the board with an MSP430 microcontroller and the radar board, which integrates the sawtooth and reference generator, radar frontend, and the baseband amplifiers, respectively. The total size of the radar system is 50 mm $\times$ 60 mm $\times$ 20 mm. As radiating subsystems, 2×2 or 4×4 patch antennas are used in the different experiments. The gain of the 2×2 array is 11.3 dB and the half-power beam width is 46°. The gain of the 4×4 array is 16.3 dB and the half-power beam width is 21.6°.

B. Coherence for the FMCW Mode

Coherence is one of the most important requirements for FMCW radars to obtain Doppler information from targets. It should be noted that the coherence mentioned in this paper is achieved by identifying the start and stop instants of each frequency ramp. An incoherent radar can only extract range profiles. Only with a coherent system, the phase history of the targets is preserved during the CPI, and Doppler information can thus be derived [29]–[31]. The mathematical expression for the beat signal within one frequency ramp interval is [28]

$$\begin{aligned} s_b(t) &= s_{TX}(t)s_{RX}^*(t) \\ &= \sigma \exp\left(j\left(\frac{4\pi\gamma R(\tau)t}{c} + \frac{4\pi f_c R(\tau)}{c} + \phi\right)\right) \end{aligned} \tag{2}$$

where $s_b(t)$ is the beat signal, $s_{TX}(t)$ is the transmitted signal, $s_{RX}^*(t)$ is the complex conjugate of the received signal, σ is the amplitude of the beat signal, $\gamma = B \times \mathrm{PRF}$ corresponds to the chirp rate, i.e., the multiplication of the transmitted bandwidth B and the ramp repetition frequency PRF [45], $R(\tau)$ represents the variation of the distance between a target and the FMCW radar, τ is the so-called "slow time," f_c is the center frequency of the frequency ramp, and c is the speed of light. Finally, ϕ is the negligible residual video phase, which can be disregarded [46].

After performing a Fourier transform to the beat signal, the frequency domain representation is

$$S_b(f) = \sigma T \exp\left(j\frac{4\pi f_c R(\tau)}{c}\right)\mathrm{sinc}\left(T\left(f - \frac{2\gamma R(\tau)}{c}\right)\right) \tag{3}$$

where T is the period of the frequency ramps.

In (3), $2\gamma R(\tau)/c$ corresponds to the beat frequency, which is proportional to the range from the radar to the target. Moreover, the slow-time phase history $\phi_d(\tau)$ in (3) is simply related to the range evolution of the target $R(\tau)$ by

$$\phi_d(\tau) = \frac{4\pi f_c R(\tau)}{c}. \tag{4}$$

Therefore, a proper slow-time range tracking of the target requires the preservation of the phase history $\phi_d(\tau)$. Great efforts should be made to control the phase in both the waveform generation and signal acquisition processes to maintain the coherence of the radar. To that purpose, it is usually needed to share the clocks at the generation and acquisition stages, which requires much more complexity in the hardware design. In this paper, the coherence property for the FMCW mode is achieved by simultaneously sampling the RPS and the baseband signal x_Q. The RPS is locked to the sawtooth signal, which is used to control the frequency of the VCO. After sampling both the RPS and the baseband signal x_Q, the synchronization procedure is performed in the digital domain to align the phase of each beat signal period. This leads to simplicity in terms of the fact that the generation and acquisition clocks can be different, i.e., the analog-to-digital converter in the audio card can work with its own clock, which is independent of that of the radar signal generator.

C. Low-IF Modulation and Envelope Detection

The audio card in a computer is used to process the signals that can be heard by humans. The human hearing range is commonly specified between 20 and 20 000 Hz [47], although there is a considerable variation between individuals. To simplify the system, the audio card usually filters

the frequencies that cannot be heard [42], including the low-frequency spectrum. Thus, there is always a high-pass filter with a cutoff frequency near 20 Hz before the sampling structure in an audio card. However, the human vital signs, i.e., respiration and heartbeat, have much lower frequency components. Note that the normal respiration rate for an adult at rest is 12 to 20 breaths/min, and the normal resting adult human heartbeat rate ranges from 60 to 100 beats/min. Hence, the frequency ranges are 0.2–0.33 and 1–1.67 Hz, respectively, which are much lower than 20 Hz and will definitely be blocked by the high-pass filter of the audio card.

For the interferometry mode, the low-IF modulation method is used to upconvert the vital signs to an IF that is higher than the aforementioned 20-Hz cutoff frequency. The schematic of the low-IF modulation is shown in Fig. 1. As observed, a pair of single-pole double-throw switches is used to connect the output paths either to ground or to the baseband signal paths through the control sequence from the microcontroller. The control frequency was set to 32 Hz in the manufactured prototype. The output signals after low-IF modulation can be expressed as follows:

$$y_I(t) = x_I(t)s_{\rm IF}(t) + V_{\rm dc}s_{\rm IF}(t) \tag{5}$$

$$y_Q(t) = x_Q(t)s_{\rm IF}(t) + V_{\rm dc}s_{\rm IF}(t) \tag{6}$$

where $V_{\rm dc}$ is the dc bias of the baseband signals produced by the baseband amplifiers, $s_{\rm IF}(t)$ is a square sequence with IF $f_{\rm IF}$ and amplitude ranging from 0 to 1, and x_I and x_Q are the baseband signals for the I and Q channels, respectively. The square sequence $s_{\rm IF}(t)$ can be further formulated using the Fourier series as indicated by

$$s_{\rm IF}(t) = 0.5 + \frac{2}{\pi}\sin(2\pi f_{\rm IF}t) + \frac{2}{3\pi}\sin(6\pi f_{\rm IF}t) + \frac{2}{5\pi}\sin(10\pi f_{\rm IF}t) + \cdots \tag{7}$$

where only the fundamental tone $2\sin(2\pi f_{\rm IF}t)/\pi$ is the wanted frequency component. The other terms, including the dc and harmonics, are filtered before sampling or just ignored during the processing. The modulated I/Q signals then become

$$y'_I(t) = A(x_I(t) + V_{\rm dc})\sin(2\pi f_{\rm IF}t) \tag{8}$$

$$y'_Q(t) = A(x_Q(t) + V_{\rm dc})\sin(2\pi f_{\rm IF}t) \tag{9}$$

where A is related to their amplitudes.

Equations (8) and (9) are the classical expressions for amplitude modulation, which can be easily demodulated by digital downconversion or envelope detection. However, since digital downconversion requires the multiplication of the modulated and carrier signals, extra synchronization would be necessary between the analog circuit and the digital low-IF demodulation to meet the coherence criteria. Therefore, envelope detection is here proposed as a more suitable choice. The envelope detection can be performed by simply squaring the modulated signals and subsequent low-pass filtering. By squaring (8) and (9), the next results are obtained

$$(y'_I(t))^2 = 0.5A^2V_{\rm dc}^2 + \underline{A^2V_{\rm dc}x_I(t)} + 0.5A^2x_I^2(t) - 0.5A^2\cos(4\pi f_{\rm IF}t)(x_I(t) + V_{\rm dc})^2 \tag{10}$$

$$(y'_Q(t))^2 = 0.5A^2V_{\rm dc}^2 + \underline{A^2V_{\rm dc}x_Q(t)} + 0.5A^2x_Q^2(t) - 0.5A^2\cos(4\pi f_{\rm IF}t)(x_Q(t) + V_{\rm dc})^2. \tag{11}$$

The underlined terms in (10) and (11) are the demodulated baseband signals. It should be noted that the $0.5A^2x_I^2(t)$ and $0.5A^2x_Q^2(t)$ summands will introduce second harmonics of the demodulated signals. Thus, to keep the fundamental signals larger than the harmonics, $V_{\rm dc}$ should be large enough. In the proposed portable hybrid radar prototype, $f_{\rm IF} = 32$ Hz and $V_{\rm dc} = 2.5$ V.

D. Vital Doppler Effect for Human Targets

The Doppler effect is the change in frequency of a wave for an observer moving relative to its source. This phenomenon has been widely used in the measurement of vehicle velocities and vital signs. If the target has mechanical vibration or rotation in addition to its bulk motion, it will induce a frequency modulation on the returned signal, which generates sidebands on the target's Doppler frequency shift. This is called the micro-Doppler effect, which can be exploited, for example, to characterize human gaits [15]. In this context, it has been reported that the micro-Doppler signature of a human target is significantly different from that of a dog [16], which gives rise to a potential radar-based application to differentiate human targets from animals.

A human subject is not completely stationary because of physiological motions such as breathing. Moreover, the reflection surface of a human target, i.e., the skin, is not a perfect conductive surface or a flat plane. Thus, a tiny motion of the human body will introduce a significant variation in the measured range profiles. In this paper, this phenomenon is referred to as the "vital Doppler" effect. The vital Doppler information is here employed to discriminate human targets from other objects.

III. Experiments With the Developed Prototype

Several experiments were carried out to demonstrate the operational capabilities and performance of the proposed portable hybrid-mode radar prototype. These experiment tests aimed at the applications of short-range localization and vital sign tracking.

A. Glass Detection and Penetration

As discussed above, the detection of transparent materials such as glass is a difficult problem for camera-based sensors. However, for microwave radar systems, detection of glass is feasible due to the different dielectric constants of air and glass. In addition, the ability to penetrate also empowers the radar to detect targets behind a glass obstacle.

This experiment was conducted to verify the detection of glass and the radar's ability to differentiate a stationary human target from other objects behind a glass. In this scenario,

Fig. 5. Experiment setup for human identification behind a glass wall.

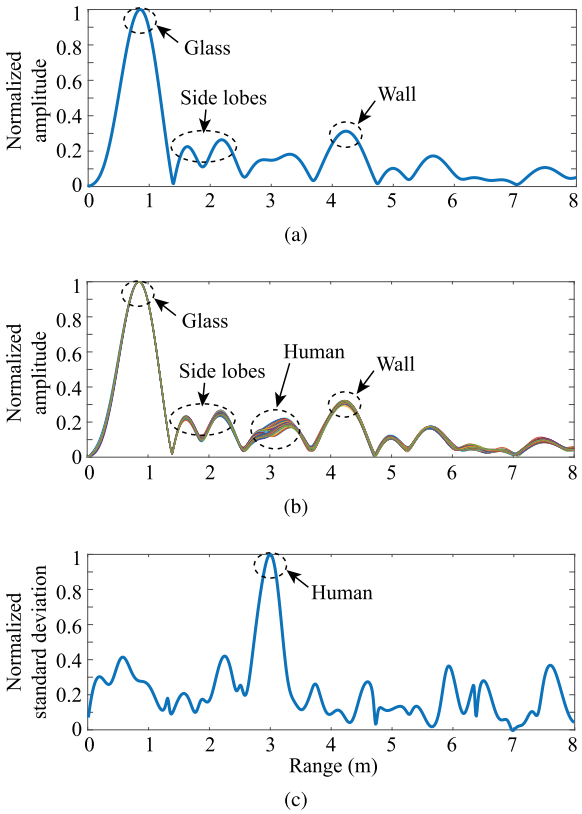

Fig. 6. Distance detection result of glass window with the human subject. (a) Range profile corresponding to the targets. (b) Several range profiles with a clear fluctuation for the human signature. (c) Isolation of the human target from the stationary glass wall.

the radar was located about 0.8 m in front of a glass wall, which had a height of 3 m and a width of more than 10 m. A human subject stood behind the glass wall, as shown in Fig. 5. Another concrete wall was also located behind the glass wall and was about 4.2 m from the radar. A pair of 4×4 patch antenna arrays, whose beam widths were 21.6°, was used as the transmitter and receiver antennas. Fig. 6(a) plots one range profile result for the environment. The signatures of the glass wall and the concrete wall are clearly shown. However, as the human body is neither flat nor a good reflector, the signature of the human subject is too weak to be observed in Fig. 6(a).

As mentioned in Section II-D, the signature for the human target has the "vital Doppler" effect, which introduces significant variation to the measured range profiles. Fig. 6(b) shows some range profiles corresponding to different measurements in 3 s. Note the large fluctuation for the signature of the human target compared with that of the glass window, even though the human target tried his best to keep stationary. By calculating the standard deviation of different measurement data during a specific time period, the human target can be identified with signatures of other stationary targets suppressed. Fig. 6(c) shows the normalized standard deviation of the measurements in Fig. 6(b). The stationary targets, i.e., the glass wall and the concrete wall, are eliminated and only the human target is observable.

B. Stationary Target Discrimination

The experimental results of Section III-A demonstrated that it is possible to differentiate a stationary human target from other stationary objects based on the "vital Doppler" effect. However, in real life, situations are always much more complicated, for example, the situation in a parking lot, where there may exist human targets, stopped cars, as well as parked cars with running engines. It becomes practical to identify human targets in such a complex environment for particular applications such as driverless vehicles.

In this experiment, the human subject stood beside a parked car with a running engine. The proposed portable radar was mounted on a tripod to do a mechanical scan in the FMCW mode. The scan step angle was 4°. Fig. 7(a) shows the photograph of the experiment setup. The engine of the white car near the human was running, being the distance between both targets of about 1.5 m.

Fig. 7(b) represents the 2-D mapping of the measured range profiles. A large echo detected at the distance of about 8 m is observable, which corresponds to the location of the car and the stationary human. The reason that these two targets that are overlapped in the 2-D mapping plot must be found in the limited antenna directivity, which corresponds to a 21.6° beamwidth. In other words, the angular resolution is not high enough to differentiate the human subject from the car. Since the radar prototype is portable, it is almost impossible to achieve an extremely narrow beamwidth with a highly constrained antenna size. The other returns on the left of Fig. 7(b) correspond to the signatures of other stopped cars in the parking lot.

Even though the angular resolution of the proposed portable radar is not high enough to differentiate the adjacent human target and the car, it is still possible to pinpoint the human subject and eliminate the other stationary clutter returns based on the human "vital Doppler" effect. After calculating the standard deviation of different measurements in each direction, the differentiated 2-D mapping in Fig. 7(c) has been obtained. Except for the human target, all the signatures of the stationary

(a)

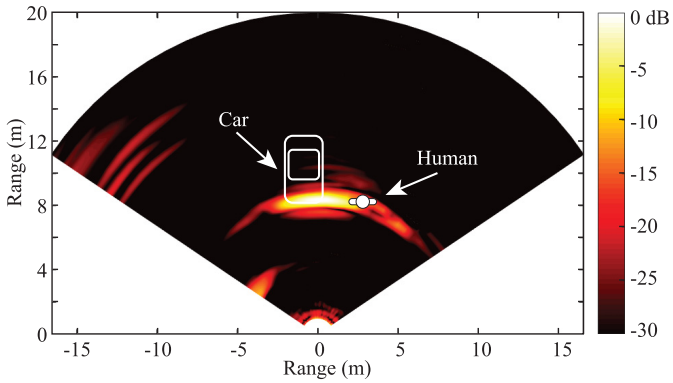

(b)

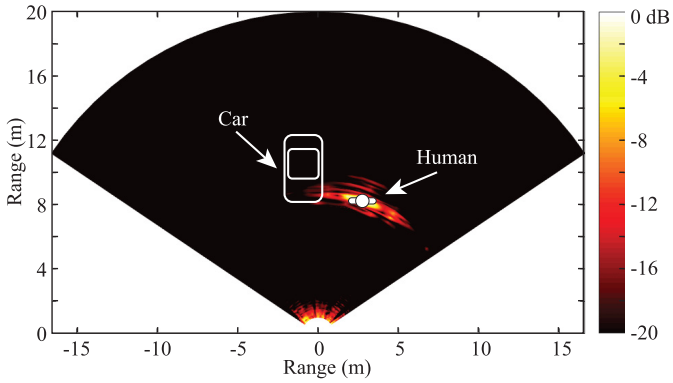

(c)

Fig. 7. (a) Experimental setup for a 2-D scan. (b) 2-D mapping result for the scenario. (c) Human target identification for the 2-D mapping experiment.

targets, including the parked car with running engine, are suppressed. This experiment reveals the ability of the proposed radar sensor to discriminate stationary human subjects in a complex environment.

C. Human Motion Tracking With ISAR

For FMCW radars, it is easy to obtain range profiles of the targets. However, in a crowded environment, such as a stock house, a home, or a clinical scenario, there are many strong stationary clutter returns, which make it difficult to find the wanted moving targets.

As addressed in Section II, a coherent FMCW radar preserves the phase history of targets during the CPI and Doppler information can thus be derived. Hence, ISAR images, which are widely used in radar imaging applications, can be formed

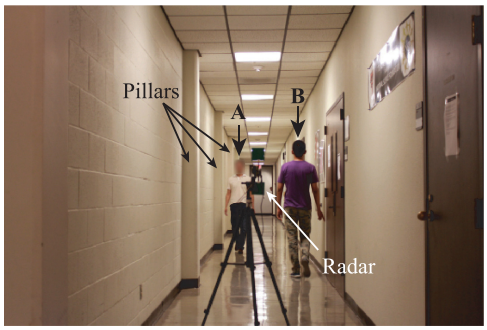

Fig. 8. Photograph of the experimental environment for ISAR video production.

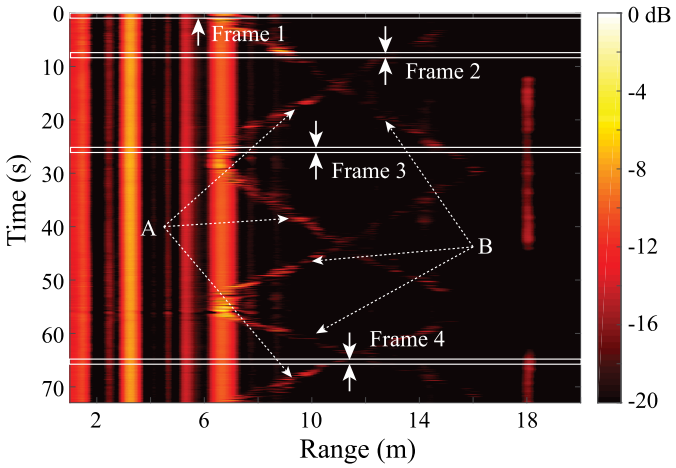

Fig. 9. Range profile matrix for two human subjects walking in opposite directions in a narrow corridor.

with the purpose of isolating the wanted moving targets from surrounding clutter.

In this experiment, the portable prototype was used to illuminate two human subjects walking in opposite directions in front of the radar in a corridor. The experiment setup is shown in Fig. 8. The corridor is quite narrow with walls and many pillars, which cause a lot of clutter returns.

Fig. 9 shows the range profile matrix for the experiment in a 73-s CPI. Many strong vertical strips, which correspond to the stationary objects, can be observed in Fig. 9. In addition, the traces of the two moving human subjects are observable, but are much weaker than the stationary clutter returns.

An ISAR image can be obtained by performing a fast Fourier transform along the slow time direction for a given slow time interval. Furthermore, a series of ISAR images can be combined together to form a video,[1] which can be used to reveal the movement properties of the targets. A frame of the ISAR video when both human subjects were stopped is detailed in Fig. 10(a) (frame 1). As a proof of the coherence of the portable hybrid radar, the zero-Doppler echoes corresponding to the stationary objects are clearly observable. Since the two human subjects were stopped at this time, both of their velocities are zero, leading to the fact that only zero-Doppler signatures are observed in this Doppler–range map.

[1]As noted in this paper, the audio card in a laptop was used to sample the data. Real-time signal processing was implemented in National Instruments LabVIEW. This material is 61.6 MB in size.

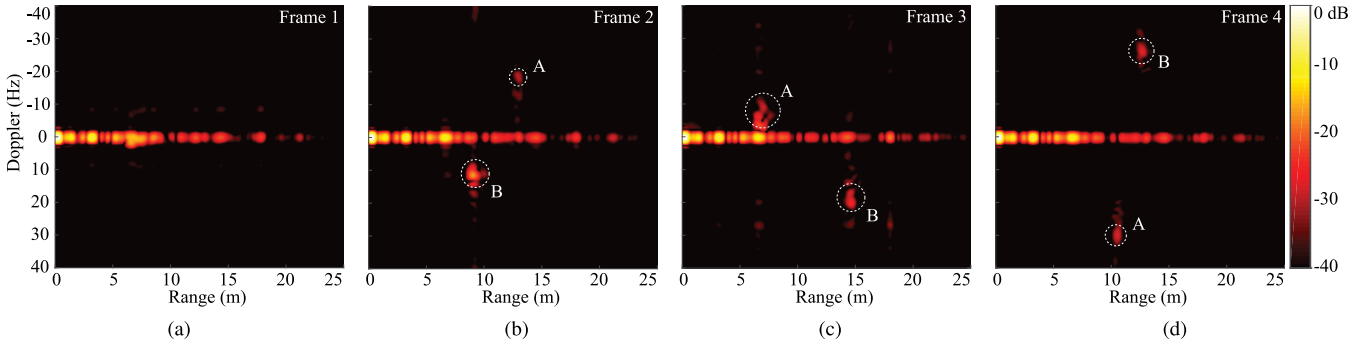

Fig. 10. (a) Frame 1 of the ISAR video at the beginning of data acquisition. (b) Frame 2 of the ISAR video at 7 s. (c) Frame 3 of the ISAR video at 26 s. (d) Frame 4 of the ISAR video at 64 s.

Fig. 10(b) plots the ISAR frame (frame 2) corresponding to the instant 7 s of the acquisition time (see Fig. 9). At that instant, subject A was walking toward the radar, while subject B was walking away from the radar. In the referred range–Doppler image, the return associated with subject A appears above the zero-Doppler strip, while subject B provides an echo below the zero-Doppler signature.

Fig. 10(c) and (d) shows the two frames of the ISAR video (frames 3 and 4) corresponding to the 26-s and 64-s instants, respectively. In relation to Fig. 10(c), subject A was close to the radar and he planned to turn around with a velocity close to zero, while subject B was still walking away from the radar system. Regarding Fig. 10(d), subject A was walking back to the radar and subject B was walking away from the radar. The echoes observed around the main signatures in Fig. 10 correspond to the micro-Doppler features of the human gaits.

The ISAR images provide the proposed portable radar with the 2-D isolation and tracking capabilities by combining the Doppler information and the absolute ranging. This could be leveraged for radar-based short-range tracking for healthcare or driverless vehicle applications.

D. Human Vital Sign Measurements Through Low-IF Modulation

It is well known that microwave interferometry radars are very sensitive to detect vital signs and that they can provide millimeter or even submillimeter scale accuracy. For the interferometry mode of the developed hybrid radar prototype, accurate respiration and heartbeat rates can be measured remotely.

In this experiment, the human subject sat about 1.5 m in front of the radar and backed the prototype. The human subject was asked to breath normally during the measurement period. As detailed in Section II, the low-IF modulation method was implemented in the radar system to upconvert the low-frequency vital signs to an IF of 32 Hz, thus avoiding the suppression of the high-pass filtering of the audio card. An envelope detection method after the acquisition stage was employed to recover the vital signs. Fig. 11(a) depicts the recorded time-domain I/Q channel signals. The vital signs were modulating a 32-Hz low-IF carrier, which is higher than the 20-Hz cutoff frequency of the audio card.

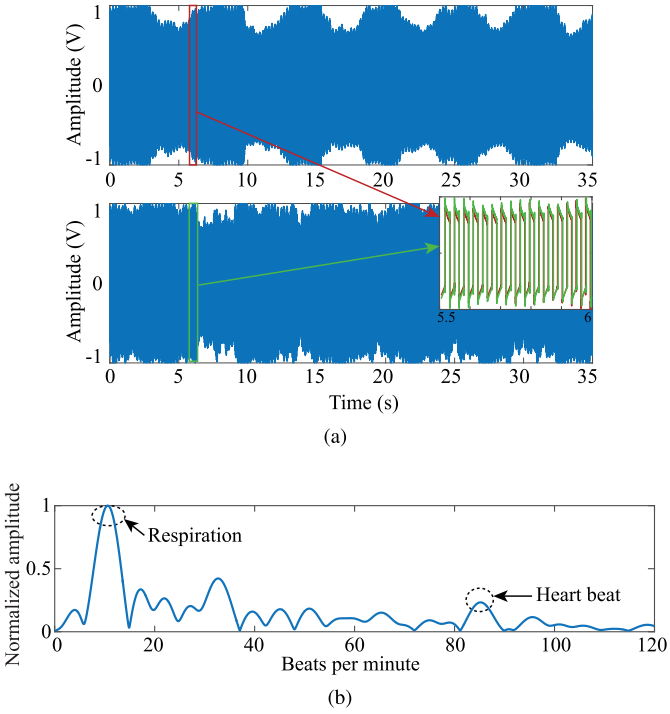

Fig. 11. (a) Time-domain I and Q channel signals. (b) Normalized frequency-domain spectrum after envelope detection.

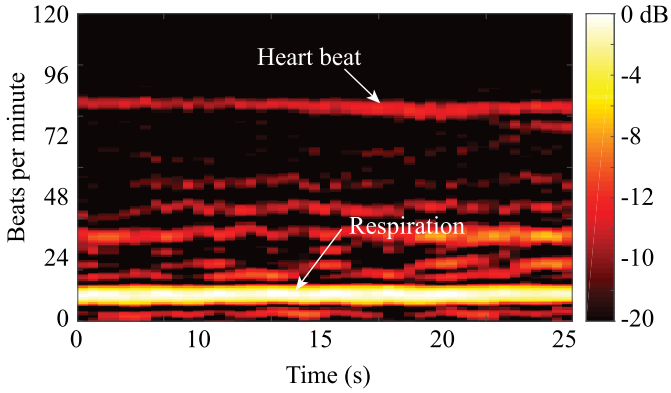

Fig. 12. Spectrogram of the vital signs after envelope detection.

Fig. 11(b) shows the normalized spectrum after envelope detection. The respiration and heartbeat rates can be clearly observed. The respiration rate of the subject was about

13 cycles/min and the heartbeat frequency was about 85 beats/min. In addition, the respiration and heartbeat can be also clearly identified in the spectrogram of the continuous measurement of Fig. 12. The two bright strips show the time evolution of the frequencies for the respiration and heartbeat.

This experiment illustrates the radar ability for accurate vital sign measurements, which can be used in remote health monitoring applications. Additionally, it should be mentioned that the detection sensitivity of vital signs is highly dependent on subjects, the body part facing the radar [48], as well as the existence of random body movement noise.

IV. Conclusion

A portable hybrid radar system for short-range localization and vital sign tracking is presented in this paper. The proposed system incorporates the FMCW mode and the interferometry (Doppler) mode, which provide the sensor with the capability of deriving absolute range information and tiny vital signs (i.e., respiration and heartbeat) of human targets. Portability and low cost are achieved through the design of the RF signal paths, the utilization of the audio card, and the implementation of the envelope detection.

Several experiments were carried out in this paper to reveal the distinct features of the proposed portable hybrid radar. They showed that the developed system can easily detect glass, which may be a challenge for optical-based sensors. In addition, 2-D scans in complex environments revealed that the hybrid sensor is able to differentiate human targets from other surrounding objects. Moreover, ISAR images were used to track the echoes of moving human targets in an environment with strong clutter returns. Finally, accurate respiration and heartbeat rates were measured for the interferometry mode, which proves the potential applications of the radar prototype in remote health monitoring and vital sign tracking. These experiments reveal the potential applications of the proposed portable and configurable radar system in multiple areas. Future work would be focused on the realization of electrical beam steering and chip level integration. In addition, the design of the proposed system does not rely on the RF frequency. It can be easily implemented with higher frequency RF transceivers with the benefits of higher resolution in the FMCW mode and higher sensitivity in the interferometry mode.

References

[1] J. Han, L. Shao, D. Xu, and J. Shotton, "Enhanced computer vision with microsoft Kinect sensor: A review," *IEEE Trans. Cybern.*, vol. 43, no. 5, pp. 1318–1334, Oct. 2013.

[2] S. Zhang and P. S. Huang, "High-resolution, real-time three-dimensional shape measurement," *Opt. Eng.*, vol. 45, no. 12, pp. 123601-1–123601-8, Dec. 2006.

[3] Y. Wang, K. Liu, Q. Hao, D. L. Lau, and L. G. Hassebrook, "Period coded phase shifting strategy for real–time 3-D structured light illumination," *IEEE Trans. Image Process.*, vol. 20, no. 11, pp. 3001–3013, Nov. 2011.

[4] Z. Zalevsky, A. Shpunt, A. Maizels, and J. Garcia, "Method and system for object reconstruction," WO Patent 2007 043 036, Apr. 19, 2007.

[5] C.-I. Chang, *Hyperspectral Imaging: Techniques for Spectral Detection and Classification*. Springer, 2003.

[6] F.-K. Wang, T.-S. Horng, K.-C. Peng, J.-K. Jau, J.-Y. Li, and C.-C. Chen, "Seeing through walls with a self-injection-locked radar to detect hidden people," in *IEEE MTT-S Int. Microw. Symp. Dig.*, Jun. 2012, pp. 1–3.

[7] Y. Wang, Q. Liu, and A. E. Fathy, "CW and pulse–Doppler radar processing based on FPGA for human sensing applications," *IEEE Trans. Geosci. Remote Sens.*, vol. 51, no. 5, pp. 3097–3107, May 2013.

[8] F. K. Wang, T. S. Horng, K. C. Peng, J. K. Jau, J. Y. Li, and C. C. Chen, "Detection of concealed individuals based on their vital signs by using a see-through-wall imaging system with a self-injection-locked radar," *IEEE Trans. Microw. Theory Techn.*, vol. 61, no. 1, pp. 696–704, Jan. 2013.

[9] X. Liu, H. Leung, and G. A. Lampropoulos, "Effect of wall parameters on ultra-wideband synthetic aperture through-the-wall radar imaging," *IEEE Trans. Aerosp. Electron. Syst.*, vol. 48, no. 4, pp. 3435–3449, Oct. 2012.

[10] C. Li, V. M. Lubecke, O. Boric-Lubecke, and J. Lin, "A review on recent advances in Doppler radar sensors for noncontact healthcare monitoring," *IEEE Trans. Microw. Theory Techn.*, vol. 61, no. 5, pp. 2046–2060, May 2013.

[11] B. Schleicher, I. Nasr, A. Trasser, and H. Schumacher, "IR-UWB radar demonstrator for ultra-fine movement detection and vital-sign monitoring," *IEEE Trans. Microw. Theory Techn.*, vol. 61, no. 5, pp. 2076–2085, May 2013.

[12] C. Gu *et al.*, "Accurate respiration measurement using DC-coupled continuous-wave radar sensor for motion-adaptive cancer radiotherapy," *IEEE Trans. Biomed. Eng.*, vol. 59, no. 11, pp. 3117–3123, Nov. 2012.

[13] Y. Kim and H. Ling, "Through-wall human tracking with multiple Doppler sensors using an artificial neural network," *IEEE Trans. Antennas Propag.*, vol. 57, no. 7, pp. 2116–2122, Jul. 2009.

[14] H. Gao, L. Xie, S. Wen, and Y. Kuang, "Micro-Doppler signature extraction from ballistic target with micro-motions," *IEEE Trans. Aerosp. Electron. Syst.*, vol. 46, no. 4, pp. 1969–1982, Oct. 2010.

[15] S. S. Ram and H. Ling, "Analysis of microDopplers from human gait using reassigned joint time-frequency transform," *Electron. Lett.*, vol. 43, no. 23, p. 1, Nov. 2007.

[16] M. Otero, "Application of a continuous wave radar for human gait recognition," *Proc. SPIE*, vol. 5809, pp. 538–548, May 2005.

[17] C. Li, X. Yu, C.-M. Lee, D. Li, L. Ran, and J. Lin, "High-sensitivity software-configurable 5.8-GHz radar sensor receiver chip in 0.13-μm CMOS for noncontact vital sign detection," *IEEE Trans. Microw. Theory Techn.*, vol. 58, no. 5, pp. 1410–1419, May 2010.

[18] A. D. Droitcour, O. Boric-Lubecke, V. M. Lubecke, and J. Lin, "0.25-μm CMOS and BiCMOS single-chip direct-conversion Doppler radars for remote sensing of vital signs," in *IEEE Int. Solid-State Circuits Conf. Tech. Dig.*, vol. 1. Feb. 2002, pp. 348–349.

[19] C. Gu, G. Wang, Y. Li, T. Inoue, and C. Li, "A hybrid radar-camera sensing system with phase compensation for random body movement cancellation in Doppler vital sign detection," *IEEE Trans. Microw. Theory Techn.*, vol. 61, no. 12, pp. 4678–4688, Dec. 2013.

[20] C. Li, J. Ling, J. Li, and J. Lin, "Accurate Doppler radar noncontact vital sign detection using the RELAX algorithm," *IEEE Trans. Instrum. Meas.*, vol. 59, no. 3, pp. 687–695, Mar. 2010.

[21] H. Rohling and C. Moller, "Radar waveform for automotive radar systems and applications," in *Proc. IEEE Radar Conf.*, May 2008, pp. 1–4.

[22] M. Mercuri, D. Schreurs, and P. Leroux, "SFCW microwave radar for in-door fall detection," in *Proc. IEEE Topical Conf. Biomed. Wireless Technol., Netw., Sens. Syst. (BioWireleSS)*, Santa Clara, CA, USA, Jan. 2012, pp. 53–56.

[23] T. Mitomo, N. Ono, H. Hoshino, Y. Yoshihara, O. Watanabe, and I. Seto, "A 77 GHz 90 nm CMOS transceiver for FMCW radar applications," *IEEE J. Solid-State Circuits*, vol. 45, no. 4, pp. 928–937, Apr. 2010.

[24] S. Scheiblhofer, S. Schuster, and A. Stelzer, "High-speed FMCW radar frequency synthesizer with DDS based linearization," *IEEE Microw. Wireless Compon. Lett.*, vol. 17, no. 5, pp. 397–399, May 2007.

[25] N. Pohl, T. Jaeschke, and K. Aufinger, "An ultra-wideband 80 GHz FMCW radar system using a SiGe bipolar transceiver chip stabilized by a fractional-N PLL synthesizer," *IEEE Trans. Microw. Theory Techn.*, vol. 60, no. 3, pp. 757–765, Mar. 2012.

[26] J. D. Park and W. J. Kim, "An efficient method of eliminating the range ambiguity for a low-cost FMCW radar using VCO tuning characteristics," *IEEE Trans. Microw. Theory Techn.*, vol. 54, no. 10, pp. 3623–3629, Oct. 2006.

[27] T. Musch, "A high precision 24-GHz FMCW radar based on a fractional-N ramp-PLL," *IEEE Trans. Instrum. Meas.*, vol. 52, no. 2, pp. 324–327, Apr. 2003.

[28] G. Wang, J. M. Muñoz-Ferreras, C. Gu, C. Li, and R. Gómez-García, "Application of linear-frequency-modulated continuous-wave (LFMCW) radars for tracking of vital signs," *IEEE Trans. Microw. Theory Techn.*, vol. 62, no. 6, pp. 1387–1399, Jun. 2014.
[29] D. A. Ausherman, A. Kozma, J. L. Walker, H. M. Jones, and E. C. Poggio, "Developments in radar imaging," *IEEE Trans. Aerosp. Electron. Syst.*, vol. AES-20, no. 4, pp. 363–400, Jul. 1984.
[30] J. L. Walker, "Range-Doppler imaging of rotating objects," *IEEE Trans. Aerosp. Electron. Syst.*, vol. AES-16, no. 1, pp. 23–52, Jan. 1980.
[31] F. Berizzi, E. D. Mese, M. Diani, and M. Martorella, "High-resolution ISAR imaging of maneuvering targets by means of the range instantaneous Doppler technique: Modeling and performance analysis," *IEEE Trans. Image Process.*, vol. 10, no. 12, pp. 1880–1890, Dec. 2001.
[32] Z. Peng, J. M. Muñoz-Ferreras, Y. Tang, R. Gómez-García, and C. Li, "Portable coherent frequency-modulated continuous-wave radar for indoor human tracking," in *Proc. IEEE Topical Conf. Biomed. Wireless Technol., Netw., Sens. Syst. (BioWireleSS)*, Austin, TX, USA, Jun. 2016, pp. 36–38.
[33] Z. Peng, J. M. Muñoz-Ferreras, R. Gómez-García, L. Ran, and C. Li, "24-GHz biomedical radar on flexible substrate for ISAR imaging," in *IEEE MTT-S Int. Wireless Symp. Dig.*, Shanghai, China, Mar. 2016, pp. 1–4.
[34] M. I. Skolnik, *Introduction to Radar Systems*, 3rd ed. New York, NY, USA: McGraw-Hill, 2002.
[35] J. Velner, E. A. M. Klumperink, B. Nauta, and F. E. van Vliet, "Multi-band linear chirp generation based on a type-III PLL," in *IEEE MTT-S Int. Microw. Symp. Dig.*, Jun. 2013, pp. 1–4.
[36] J. Lee, Y.-A. Li, M.-H. Hung, and S.-J. Huang, "A fully-integrated 77-GHz FMCW radar transceiver in 65-nm CMOS technology," *IEEE J. Solid-State Circuits*, vol. 45, no. 12, pp. 2746–2756, Dec. 2010.
[37] A. Anghel, G. Vasile, R. Cacoveanu, C. Ioana, and S. Ciochina, "Short-range wideband FMCW radar for millimetric displacement measurements," *IEEE Trans. Geosci. Remote Sens.*, vol. 52, no. 9, pp. 5633–5642, Sep. 2014.
[38] P. V. Brennan, Y. Huang, M. Ash, and K. Chetty, "Determination of sweep linearity requirements in FMCW radar systems based on simple voltage-controlled oscillator sources," *IEEE Trans. Aerosp. Electron. Syst.*, vol. 47, no. 3, pp. 1594–1604, Jul. 2011.
[39] A. Meta, P. Hoogeboom, and L. P. Ligthart, "Signal processing for FMCW SAR," *IEEE Trans. Geosci. Remote Sens.*, vol. 45, no. 11, pp. 3519–3532, Nov. 2007.
[40] D. R. Wehner, *High-Resolution Radar*, 2nd ed. Boston, MA, USA: Artech House, 1995.
[41] G. Wang, C. Gu, T. Inoue, and C. Li, "A hybrid FMCW-interferometry radar for indoor precise positioning and versatile life activity monitoring," *IEEE Trans. Microw. Theory Techn.*, vol. 62, no. 11, pp. 2812–2822, Nov. 2014.
[42] A. Carullo, M. Parvis, and A. Vallan, "An audio card-based kit for educational purposes," *IEEE Trans. Instrum. Meas.*, vol. 52, no. 3, pp. 733–737, Jun. 2003.
[43] X. Zhao, C. Song, V. Lubecke, and O. Boric-Lubecke, "DC coupled Doppler radar physiological monitor," in *Proc. 33rd Annu. Int. Conf. IEEE Eng. Med. Biol. Soc.*, Boston, MA, USA, Aug./Sep. 2011, pp. 1909–1912.
[44] C. Gu and C. Li, "DC coupled CW radar sensor using fine-tuning adaptive feedback loop," *Electron. Lett.*, vol. 48, no. 6, pp. 344–345, Mar. 2012.
[45] J. M. Muñoz-Ferreras and R. Gómez-García, "A deramping-based multiband radar sensor concept with enhanced ISAR capabilities," *IEEE Sensors J.*, vol. 13, no. 9, pp. 3361–3368, Sep. 2013.
[46] W. G. Carrara, R. S. Goodman, and R. M. Majewski, *Spotlight Synthetic Aperture Radar: Signal Processing Algorithms*. Boston, MA, USA: Artech House, 1995.
[47] M. Schroeder, T. D. Rossing, F. Dunn, W. M. Hartmann, D. M. Campbell, and N. H. Fletcher, *Springer Handbook of Acoustics*. Berlin, Germany: Springer, 2007.
[48] C. Li, Y. Xiao, and J. Lin, "Experiment and spectral analysis of a low-power Ka-band heartbeat detector measuring from four sides of a human body," *IEEE Trans. Microw. Theory Techn.*, vol. 54, no. 12, pp. 4464–4471, Dec. 2006.

Zhengyu Peng (S'15) received the B.S. and M.Sc. degrees in electrical engineering from Zhejiang University, Hangzhou, China, in 2011 and 2014, respectively. He is currently pursuing the Ph.D. degree in electrical engineering at Texas Tech University, Lubbock, TX, USA.

His current research interests include antennas, microwave circuits, and biomedical application of microwave and RF circuits and systems.

José-María Muñoz-Ferreras (M'15) received the degree in telecommunication engineering and Ph.D. degree in electrical and electronic engineering from the Polytechnic University of Madrid, Madrid, Spain, in 2004 and 2008, respectively.

He is currently with the Department of Signal Theory and Communications, University of Alcalá, Alcalá de Henares, Madrid. His current research interests include radar signal processing, advanced radar systems and concepts, and microwave and RF circuits and systems, specifically focusing on high-resolution inverse synthetic aperture radar images, and the design and validation of radar systems for short-range applications.

Dr. Muñoz-Ferreras is a reviewer for several IEEE and IET publications. He serves as a member of the Technical Review Board for the IEEE International Geoscience and Remote Sensing Symposium and the IEEE Radar Conference.

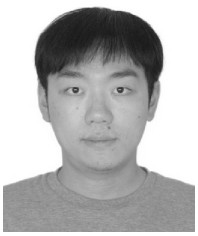

Yao Tang (S'15) received the B.S. degree from the University of Electronic Science and Technology of China, Chengdu, China, in 2011. He is currently pursuing the Ph.D. degree in electrical engineering at Texas Tech University (TTU), Lubbock, TX, USA.

He is currently with the Department of Electrical and Computer Engineering, TTU. His current research interests include microwave and RF wireless sensors and millimeter-wave radar-system design.

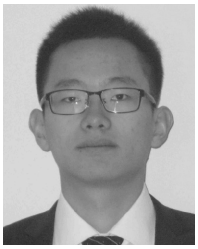

Chenhui Liu (S'15) received the B.S. degree in optoelectronics information engineering from the Huazhong University of Science and Technology, Wuhan, China, in 2013, and the M.Sc. degree in electrical engineering from Texas Tech University, Lubbock, TX, USA, in 2015.

He is currently with Qualcomm, San Jose, CA, USA. His current research interests include analog and RF system design and application.

Roberto Gómez-García (S'02–M'06–SM'11) was born in Madrid, Spain, in 1977. He received the degree in telecommunication engineering and Ph.D. degree in electrical and electronic engineering from the Polytechnic University of Madrid, Madrid, in 2001 and 2006, respectively.

Since 2006, he has been an Associate Professor with the Department of Signal Theory and Communications, University of Alcalá, Alcalá de Henares, Madrid. He has been, for several research stays, with the C2S2 Department, XLIM Research Institute (formerly IRCOM), University of Limoges, Limoges, France, the Telecommunications Institute, University of Aveiro, Aveiro, Portugal, the U.S. Naval Research Laboratory, Microwave Technology Branch, Washington, DC, USA, and Purdue University, West Lafayette, IN, USA. His current research interests include the design of fixed/tunable high-frequency filters and multiplexers in planar, hybrid and monolithic microwave integrated circuit technologies, multifunction circuits and systems, and software-defined radio and radar architectures for telecommunications, and remote sensing and biomedical applications.

Dr. Gómez-Garcí serves as a member of the Technical Review Board for several IEEE and EuMA conferences. He is also a member of the IEEE MTT-S Filters and Passive Components (MTT-8), IEEE MTT-S Biological Effect and Medical Applications of RF and Microwave (MTT-10), IEEE MTT-S Wireless Communications (MTT-20), and IEEE CAS-S Analog Signal Processing Technical Committees. He is an Associate Editor of the IEEE TRANSACTIONS OF MICROWAVE THEORY AND TECHNIQUES, IEEE TRANSACTIONS ON CIRCUITS AND SYSTEMS—I: REGULAR PAPERS, and *IET Microwaves, Antennas, and Propagation*. He was a Guest Editor of the 2013 IEEE JOURNAL ON EMERGING AND SELECTED TOPICS IN CIRCUITS AND SYSTEMS "Special Issue on Advanced Circuits and Systems for CR/SDR Applications," *IET Microwaves, Antennas, and Propagation* 2013 "Special Issue on Advanced Tuneable/Reconfigurable and Multifunction RF/Microwave Filtering Devices," and the *IEEE Microwave Magazine* 2014 "Special Issue on Recent Trends on RF/Microwave Tunable Filter Design." He is a reviewer for several IEEE, IET, EuMA, and Wiley journals.

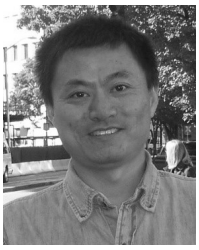

Lixin Ran received the B.S., M.S., and Ph.D. degrees from Zhejiang University, Hangzhou, China, in 1991, 1994, and 1997, respectively.

He was an Assistant Professor, an Associate Professor, and a Full Professor with the Department of Information and Electronics Engineering, Zhejiang University, in 1997, 1999, and 2004, respectively. He is currently the Director of the Laboratory of Applied Research on Electromagnetics, Zhejiang University. In 2005, 2009 and 2012, he visited the Massachusetts Institute of Technology, Cambridge, MA, USA, as a Visiting Scientist. He has co-authored over 120 research papers published in peer-reviewed journals. He is the inventor of over 30 licensed patents. His current research interests include new concept antennas, radio-aware sensing and imaging, radio frequency, microwave and terahertz systems, and artificial active media.

Changzhi Li (S'06–M'09–SM'13) received the B.S. degree in electrical engineering from Zhejiang University, Hangzhou, China, in 2004, and the Ph.D. degree in electrical engineering from the University of Florida, Gainesville, FL, USA, in 2009.

From 2007 to 2009, he was with Alereon Inc., Austin, TX, USA, and Coherent Logix Inc., Austin, where he was involved in ultra-wideband transceivers and software-defined radio. In 2009, he joined Texas Tech University, Lubbock, TX, USA, as an Assistant Professor, and became an Associate Professor in 2014. His current research interests include biomedical applications of microwave/RF, wireless sensor, and analog circuits.

Dr. Li was the recipient of the IEEE MTT-S Graduate Fellowship Award in 2008, the NSF Faculty Early CAREER Award in 2013, the ASEE Frederick Emmons Terman Award in 2014, and the IEEE-HKN Outstanding Young Professional Award in 2014. He was the recipient of a few Best Paper Awards as author/advisor in IEEE sponsored conferences. He is an Associate Editor of the IEEE TRANSACTIONS ON CIRCUITS AND SYSTEMS—I: REGULAR PAPERS. He served as a TPC Co-Chair of the IEEE Wireless and Microwave Technology Conference in 2012 and 2013, and an Associate Editor of the IEEE TRANSACTIONS ON CIRCUITS AND SYSTEMS—II: EXPRESS BRIEFS in 2014 and 2015.